PHYSICAL REVIEW B **89**, 205413 (2014)

Substrate-induced cross-plane thermal propagative modes in few-layer graphene

Yuxiang Ni,[1] Yuriy A. Kosevich,[1,2,*] Shiyun Xiong,[1] Yann Chalopin,[1] and Sebastian Volz[1,†]
[1]*Laboratoire d'Energétique Moléculaire et Macroscopique, CNRS UPR 288, Ecole Centrale Paris, Grande Voie des Vignes, 92295 Châtenay-Malabry, France*
[2]*Semenov Institute of Chemical Physics, Russian Academy of Sciences, Kosygin str. 4, 119991 Moscow, Russia*

(Received 16 September 2013; published 12 May 2014)

We report the layer-number dependence of the averaged interlayer thermal resistances (R_{int}) of the suspended and supported few-layer graphene (FLG), simulated by equilibrium molecular dynamics (EMD). The existence of a silicon dioxide substrate significantly decreases the R_{int} of FLG at low layer number. We use the model of long-wavelength dynamics of a nanolayer adsorbed on a deformable crystal [Kosevich and Syrkin, Phys. Lett. A **135**, 298 (1989)] to explain the appearance of the substrate-induced gaps in the FLG dispersion curves and phonon radiation into the deformable substrate from these gap modes. The enhanced thermal conductance in the cross-plane direction is ascribed to the phonon radiation from FLG into the deformable substrate, which partially transfers the flow of phonon energy in FLG from the in-plane to the cross-plane direction and to the substrate. To confirm this, we calculate the cross-plane thermal resistance of three-layer graphene supported by an effective SiO_2 substrate in which atomic masses are increased by a factor of 1000. This makes the substrate almost immovable and suppresses phonon radiation from the supported FLG by complete phonon reflection at the interface. The cross-plane thermal resistance of three-layer graphene supported on such a substrate is found to be the same as its suspended counterpart.

DOI: 10.1103/PhysRevB.89.205413 PACS number(s): 65.80.Ck, 63.22.Rc, 68.65.Pq

Since its discovery, graphene has garnered great interest due to its many remarkable physical properties [1–4], among which its high in-plane thermal conductivity has been suggested as a key advantage for applications in microelectronics and thermal management [5,6]. However, the exotic properties of monolayer graphene are not always beneficial for the realization of graphene devices or interconnects and, in many cases, few-layer graphene (FLG) has more favorable properties for practical applications [7]. Contrary to its in-plane counterpart, however, the cross-plane thermal conductivity of FLG is supposed to be much lower due to the weak van der Waals interaction between layers. This strongly limits the heat-dissipation efficiency of FLG-based thermal materials. The basal plane conduction property also notably depends on the weak van der Waals cross-plane interactions that reduce the interlayer scattering [8]. As a result, knowledge of the cross-plane thermal properties of FLG becomes essential in understanding the thermal mechanisms at play in FLG.

Several works have studied the cross-plane thermal properties of suspended FLG, including a nonequilibrium molecular dynamics (NEMD) study [9] and a Debye model calculation [10]. They found a decrease in interlayer thermal resistances of FLG for increasing layer number. For supported FLG, despite a large number of studies on the in-plane thermal properties [11–13], how the heat propagates across the layers has rarely been reported.

In this paper, we present the calculation of the averaged interlayer thermal resistances R_{int} of FLG in both supported and suspended configurations by equilibrium MD simulations. We show that R_{int} in suspended FLG decreases with increasing layer number and that the SiO_2 substrate can decrease the thermal resistance and enhance the effective cross-plane thermal conductivity. The model of long-wavelength dynamics of a nanolayer adsorbed on a deformable crystal [14,15] and the sound-cone concept are introduced to explain the substrate effects on the flexural modes and the corresponding changes in energy transfer.

In the MD simulations, suspended armchair graphene layers (3 × 3.7 nm) and that supported on an amorphous SiO_2 (3 × 3.7 × 2 nm) with periodic boundary conditions in the x and y directions were chosen in this study (see Fig. 1). The finite-size effect was checked by using graphene sheets with larger cross-sectional area (6 × 6 nm, 7 × 7 nm, and 8 × 8 nm). Similar substrate thicknesses have been used previously in thermal simulations [16,17]. Amorphous SiO_2 which complies with the periodic boundary condition of the graphene domain is prepared by following the heating-quenching recipe used by Ong *et al.* [17].

EMD simulations were conducted using the LAMMPS software package [18]. The adaptive intermolecular reactive empirical bond-order (AIREBO) potential [19] was adopted to simulate FLG; this potential has been widely used to describe the carbon-carbon interactions in graphene and carbon nanotubes [20–22]. A modified Tersoff potential was used to describe Si-Si, Si-O, and O-O interactions in silica [23]. The Lennard–Jones (LJ) potential was adopted for interlayer interactions in FLG and the interfacial interactions between FLG and silica, with $\epsilon_{\text{C-C}} = 2.39$ meV, $\epsilon_{\text{Si-C}} = 8.909$ meV, $\epsilon_{\text{O-C}} = 3.442$ meV, $\sigma_{\text{C-C}} = 3.410$ Å, $\sigma_{\text{Si-C}} = 3.326$ Å, and $\sigma_{\text{O-C}} = 3.001$ Å [17,24]. The cutoff radius of the LJ potential for the Si-C and O-C interactions was set equal to 2.5σ [17]. The structure was relaxed first in the isothermal-isobaric (NPT) ensemble and then in the canonical ensemble (NVT) for 600 ps. Atomic trajectories were then calculated in the microcanonical ensemble (NVE) at 300 K. At least twenty ensemble averages were considered for each thermal resistance point.

The cross-plane thermal resistance R_c of FLG can be calculated from the following equation, which can be derived

---

[*] yukosevich@gmail.com

[†] sebastian.volz@ecp.fr

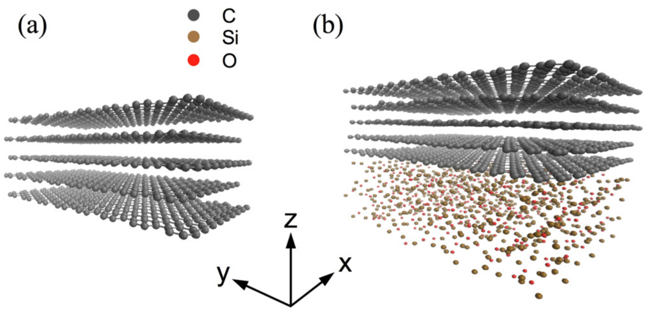

FIG. 1. (Color online) Spatial configuration of (a) five-layer suspended graphene and (b) five-layer graphene supported on a SiO_2 substrate.

from the Green–Kubo formula [25]:

$$\frac{1}{R_c} = \frac{1}{Ak_BT^2}\int_0^{+\infty}\langle p_c(0)p_c(t)\rangle dt. \tag{1}$$

The averaged interlayer thermal resistance of FLG, R_{int}, is set equal to R_c divided by the number of these mean resistances. This number is $N-1$, where N is the number of layers, yielding

$$\frac{1}{R_{\text{int}}} = \frac{N-1}{Ak_BT^2}\int_0^{+\infty}\langle p_c(0)p_c(t)\rangle dt. \tag{2}$$

The brackets denote the cross-plane heat-power autocorrelation function, k_B is the Boltzmann constant, A is the cross-section area of the FLG, and T is the equilibrium temperature. The Green–Kubo approach was used for calculating the Kapitza resistance, as for solid-liquid interfaces [26] and superlattices [27,28], by considering the fluctuating heat power across the interface. In the same manner, it is possible to use the fluctuation-dissipation theorem to express the thermal resistance of a thick system as proposed in Eq. (1) [29]. Thus the averaged interlayer resistance of a FLG system can be calculated if the total cross-plane heat power p_c of FLG is taken into account. The heat power p_c is the product of the cross-plane component of the heat flux q_c and the cross-section area A:

$$p_c = Aq_c. \tag{3}$$

For an N-atom solid system, the heat flux $\mathbf{q}(t)$ is expressed as [30]

$$\mathbf{q}(t) = \frac{1}{V}\left\{\sum_{i=1}^{N}\sum_{j=1,j\neq i}^{N}\left[\frac{1}{2}\mathbf{r}_{ij}(\mathbf{F}_{ij}\cdot\mathbf{v}_i) + \frac{1}{6}\sum_{k=1,k\neq i,j}(\mathbf{r}_{ij}+\mathbf{r}_{ik})(\mathbf{F}_{ijk}\cdot\mathbf{V}_i)\right]\right\}, \tag{4}$$

where $\mathbf{r}_{ij}$ is the interatomic distance, $\mathbf{v}_i$ is the atomic velocity, and $\mathbf{F}_{ij}$ is the interatomic force. The first term is the two-body contribution while the second term is the three-body contribution. Note that Eq. (4) takes into account only the atoms in FLG.

Figure 2 compares the calculated values of R_{int} of both suspended and supported FLG configurations. For suspended FLG, there is a drastic R_{int} jump when the layer number increases from two to four, which may be due to the change in the number of interacting layers. The cutoff radius of the LJ potential is set to 10.2 Å, within which a larger layer number brings more interacting layers and increases the interlayer phonon coupling. For FLG with layer number larger than four, the R_{int} decrease is mainly due to the size effect in the cross-plane direction, which could be eliminated with a sufficient number of layers for which R_{int} approaches the graphite limit. A similar tendency was reported in Ref. [32], where the inter-FLG resistance was found to decrease against the total layer number. Unlike in suspended FLG, no significant layer dependence is found for R_{int} in supported FLG, indicating that it is less sensitive to the layer number due to the existence of the substrate. At small layer numbers, R_{int} in supported FLG is much lower than that in the suspended configuration. These results suggest that one can reduce R_{int} in suspended FLG either by increasing the graphene layer number or by adding a substrate.

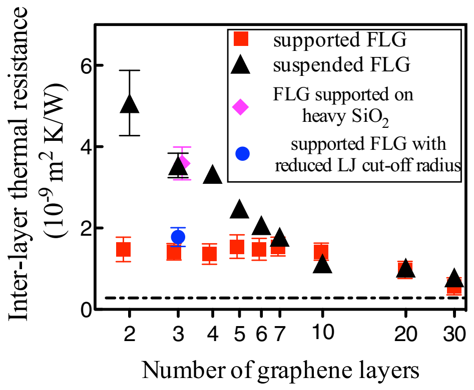

FIG. 2. (Color online) Averaged cross-plane thermal resistance of suspended and supported FLG versus layer number at 300 K. The dashed line is the resistance between neighboring layers in graphite summarized from Ref. [31]. The blue symbol refers to the case where the LJ cutoff radius includes only one graphene layer. The magenta symbol refers to an effective SiO_2 substrate in which atomic masses are increased by a factor of 1000.

Koh *et al.* [33] measured the thermal conductance of Au/Ti/FLG/SiO_2 interfaces, and the corresponding resistance is around 4×10^{-8} m^2 K/W, which is one order of magnitude larger than what is shown in Fig. 2. This is not a one-to-one comparison because the FLG/SiO_2 contact resistance is predominant in the measured results and it is in the range of $\sim10^{-8}$ m^2 K/W, as is shown in various measurements [34–36] and simulations [37,38].

The phonon dispersion relations are calculated to better understand the cross-plane thermal properties in suspended and supported FLG.

The phonon dispersion relation can be obtained from the mode kinetic energy in reciprocal space. For a given polarization, $p = x$, y, or z, the reciprocal-space representation of the velocity for atom i at time t is [39,40]

$$v_{i,k}^p(t) = v_i^p(t)e^{-ikr_i(t)}, \tag{5}$$

and the per-atom kinetic energy in reciprocal space is

$$E_{i,c}^p(k,t) = \frac{mv_{i,k}^p(t)v_{i,k}^{p*}(t)}{2}. \tag{6}$$

By Fourier transforming the atomic kinetic energy, the eigenfrequencies for a given wave vector k and the corresponding

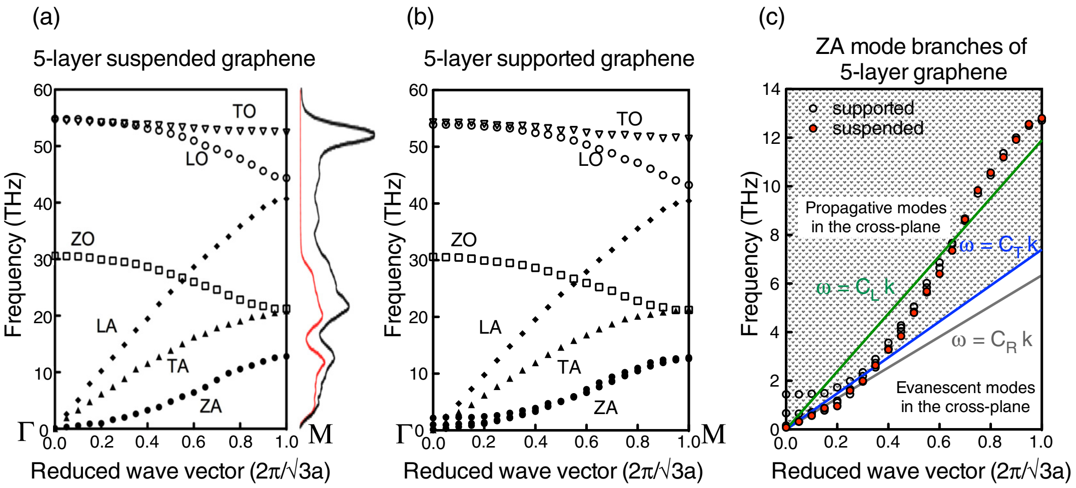

FIG. 3. (Color online) (a) Dispersion relation of five-layer suspended graphene. The spectra of phonon density of states calculated from all modes (all velocity components, black line) and only from flexural modes (cross-plane direction velocity, red line) are also shown. (b) Dispersion relation of five-layer supported graphene. (c) Flexural modes (ZA modes) branches of suspended and supported five-layer graphene with longitudinal and transverse sound lines: in the gray patterned region, graphene modes are coupled with the propagative modes of the substrate. The surface Rayleigh wave dispersion is shown as the gray line.

amplitudes of the mode kinetic energy can be found:

$$E_c^p(k,\omega) = \frac{m\left|\sum_i \int_{-\infty}^{+\infty} v_i^p(t)e^{-ikr(t)}e^{i\omega t}dt\right|^2}{2}. \qquad (7)$$

The transverse and longitudinal branches of the dispersion relation are obtained by changing the polarization of the velocities. Twenty unit cells of graphene were modeled along the wave-vector direction. Figures 3(a) and 3(b) show the dispersion-relation curves of suspended and supported five-layer graphene; a in the figure equals 2.456 Å. The spectra of phonon density of states (DOS) calculated from all modes and only from flexural modes are also shown. DOS was calculated from the time correlation function of the atomic velocities in the Fourier space.

According to Fig. 3(a), the main contribution to the spectrum of DOS below 15 THz is given by flexural modes (ZA modes). The large density of these low-frequency ZA modes ensures their dominant contribution to the in-plane thermal conductivity [41]. However, when FLG is supported on a SiO_2 substrate, two flat ZA-mode branches appear, which are shown in detail in Fig. 3(c). The flat slopes of ZA-mode branches in supported FLG indicate a low or zero propagation velocity. Those modes are confined and their contribution to the in-plane thermal conductivity is restrained. The faded in-plane thermal conductivity of supported FLG was indeed observed in many studies [12,33,42].

The observed dispersion relation of ZA modes in supported FLG is consistent with the model proposed by Kosevich and Syrkin [14,15], in which the vibrational spectra of an adsorbed nanolayer either strongly or weakly bonded with a deformable crystal were studied theoretically. In this model, the phonon spectrum of the adsorbed nanolayer, strongly bonded with the deformable substrate, is characterized by the presence of gapless surface waves with the Rayleigh-wave polarization, i.e., the surface modes of the absorbed nanolayer move in phase with the Rayleigh waves in the substrate. A linear (acoustic) dispersion was found in the long-wavelength domain. Similar results were obtained in Ref. [13], where the strong coupling between the flexural modes of graphene with surface waves of the substrate has been shown to lead to a hybridized linear dispersion in the small-wave-vector region. For the nanolayer, which is weakly bonded to the substrate, the dispersion curves both for the gapless modes with the Rayleigh-wave polarization and for the gap modes were predicted in the long-wavelength region [14,15]. An exact agreement is obtained with the present calculations for supported FLG.

The concept of a sound cone on a deformable substrate can be used to explain the effects of the low-frequency gaps in the vibrational spectra of FLG on the reduction of R_{int}, as is shown in Fig. 3(c). The longitudinal and transverse sound lines were calculated from $\omega = C_\alpha k$, where C_α corresponds either to longitudinal C_L or to transverse C_T sound velocity in SiO_2, which are set to 5950 and 3740 m/s, respectively [43]. The Rayleigh velocity C_R, approximated from the slope of the dispersion curve in the low-wave-vector domain, equals $0.88C_T$, which is a reasonable value in the typical range of $0.87C_T$ to $0.96C_T$, depending on Poisson's ratio [44]. According to Fig. 3(c), the transverse sound line divides the wave-vector–frequency plane into two regions: the one above the transverse sound line is patterned with gray dots, and the one below is blank. The wave vector k in graphene could be decomposed into components parallel and perpendicular to the plane, $k_\parallel$ and $k_\perp$: $k^2 = (\omega/C_\alpha)^2 = k_\parallel^2 + k_\perp^2$. For $k_\parallel^2 \ll (\omega/C_\alpha)^2$, $k_\perp$ is real and contributes to the *oblique* propagation of the plane wave: $u = u_0 e^{i(k_\perp r_\perp + k_\parallel r_\parallel - \omega t)}$, where $r_\parallel$ and $r_\perp$ are the positions. This corresponds to the gray patterned region above the transverse sound line. On the contrary, for $k_\parallel^2 \gg (\omega/C_\alpha)^2$, $k_\perp$ is imaginary and the corresponding wave is the evanescent surface wave with the *in-plane* propagation, $u = u_0 e^{-|k_\perp| r_\perp} e^{i(k_\parallel r_\parallel - \omega t)}$, which exponentially decays in the cross-plane direction. This corresponds to blank region below the transverse sound line.

TABLE I. Averaged interlayer thermal resistance of three-layer graphene supported on SiO_2 with modified potential depth ϵ of the Lennard–Jones potential between graphene and SiO_2.

	ϵ	2ϵ	5ϵ	10ϵ	20ϵ
$R_{\rm int}(\times 10^{-9}\ {\rm m^2\,K/W})$	1.41	1.23	0.83	0.51	0.17

By moving the graphene layer along the z direction of the graphene-SiO_2 LJ potential in the harmonic regime and recording the corresponding force change, we can find the coupling constant between the monolayer and the substrate which, together with the monolayer surface mass density, determines the perpendicular vibration frequency of the bonded monolayer in the model [14,15] and yields the corresponding frequency for graphene-SiO_2 as 1.70 THz. It is exactly the higher frequency of the modes at $k_\parallel = 0$, as is shown in Fig. 3(c). This value is validated in Ref. [38], in which the frequency of the uniform, with $k_\parallel = 0$, perpendicular graphene-SiO_2 vibrations is calculated to be 1.65 THz.

Judging from Fig. 3(c), when FLG is supported on a SiO_2 substrate, the formation of the band gaps brings more ZA modes into the gray patterned regions above the sound lines. In this region, the gap modes of FLG are propagating modes [45] in the cross-plane direction and radiate phonon energy into the substrate. Thus, the in-plane flow of phonon energy in FLG will be partly transferred into the cross-plane flow and to the energy flow into the substrate. The enhancement of the cross-plane thermal conductance of the supported FLG can be understood from the Green–Kubo formula (2): the autocorrelation function of the additional equilibrium fluctuational heat currents generated by phonon radiation into (and from) the substrate gives a positive contribution to the cross-plane thermal conductance.

To verify this conclusion, we calculate the cross-plane resistance of three-layer graphene supported on an effective SiO_2 substrate in which atomic masses are increased by a factor of 1000. This makes the substrate almost immovable and fixed and suppresses phonon radiation from the supported FLG by almost complete phonon reflection at the interface between materials with very strong mismatch both in elastic impedances and in phonon spectra [15]. In this system we obtain the same value of the cross-plane thermal resistance as for the suspended three-layer graphene; see Fig. 2. This result confirms unambiguously that just phonon radiation into the deformable substrate makes the difference between cross-plane thermal resistances of the supported and suspended FLG.

The importance of the phonon radiation into the deformable substrate is also confirmed by changing the strength of the LJ potential between the FLG and SiO_2 substrate: The cross-plane resistance continuously decreases with the potential-depth increase by an order of magnitude for the twenty-fold increase of the LJ potential depth ϵ; see Table I. The increase of the cutoff radius of the LJ potential between the FLG and SiO_2 substrate, from one to two graphene layers, which opens a new channel of phonon energy transfer into the substrate, also results in a decrease in cross-plane resistance from 1.78 to $1.41 \times 10^9\ {\rm m^2\,K/W}$; see Fig. 2. This result also confirms the contribution of phonon radiation into the deformable substrate to the difference between the cross-plane thermal resistances of supported vs suspended FLG.

We would like to emphasize also that the substrate-induced gaps in the calculated dispersion curves and corresponding frequencies for the *in-plane* dynamics are in satisfactory agreement with the prediction of the Frenkel–Kontorova model, which describes the phonon dispersion relation of a linear chain of particles bonded to a *fixed* periodic substrate potential [46]. But as we conclude above, the coupling to the fixed, phonon-free, Frenkel–Kontorova-like substrate does change the *cross-plane* thermal resistance of the supported FLG. To describe and understand the difference between the cross-plane thermal resistances of the supported and suspended FLG, one needs to develop the model of long-wavelength dynamics of a nanolayer adsorbed on a *deformable* crystal, like the model which was developed in Refs. [14,15].

In summary, by using molecular dynamics simulations, we show that the cross-plane thermal resistance in suspended FLG decreases with the layer number, and the SiO_2 substrate could significantly decrease the cross-plane thermal resistance of FLG with low layer number. Phonon dispersion curves show the existence of substrate-induced gaps in the spectrum of ZA modes of the supported FLG. The enhanced thermal conductance in the cross-plane direction was ascribed to the additional fluctuational cross-plane heat currents generated by phonon radiation from FLG into the deformable substrate. The obtained results are important for FLG applications in microelectronics, interconnects, and thermal-management structures.

---

[1] S. V. Morozov, K. S. Novoselov, M. I. Katsnelson, F. Schedin, D. C. Elias, J. A. Jaszczak, and A. K. Geim, Phys. Rev. Lett. **100**, 016602 (2008).

[2] S. Ghosh, I. Calizo, D. Teweldebrhan, E. P. Pokatilov, D. L. Nika, A. A. Balandin, W. Bao, F. Miao, and C. N. Lau, Appl. Phys. Lett. **92**, 151911 (2008).

[3] D. L. Nika, S. Ghosh, E. P. Pokatilov, and A. A. Balandin, Appl. Phys. Lett. **94**, 203103 (2009).

[4] V. E. Dorgan, M.-H. Bae, and E. Pop, Appl. Phys. Lett. **97**, 082112 (2010).

[5] J. H. Seol, I. Jo, A. L. Moore, L. Lindsay, Z. H. Aitken, M. T. Pettes, X. Li, Z. Yao, R. Huang, D. Broido, N. Mingo, R. S. Ruoff, and L. Shi, Science **328**, 213 (2010).

[6] W. Jang, Z. Chen, W. Bao, C. N. Lau, and C. Dames, Nano Lett. **10**, 3909 (2010).

[7] Y. K. Koh, M.-H. Bae, D. G. Cahill, and E. Pop, ACS Nano **5**, 269 (2010).

[8] D. L. Nika, E. P. Pokatilov, and A. A. Balandin, Phys. Status Solidi B **248**, 2609 (2011).

[9] Z. Y. Wei, Z. H. Ni, K. D. Bi, M. H. Chen, and Y. F. Chen, Phys. Lett. A **375**, 1195 (2011).

[10] K. Sun, M. A. Stroscio, and M. Dutta, Superlattices Microstruct. **45**, 60 (2009).

[11] L. Lindsay, D. A. Broido, and N. Mingo, Phys. Rev. B **83**, 235428 (2011).
[12] Z. Wang, R. Xie, C. T. Bui, D. Liu, X. Ni, B. Li, and J. T. L. Thong, Nano Lett. **11**, 113 (2010).
[13] Z.-Y. Ong and E. Pop, Phys. Rev. B **84**, 075471 (2011).
[14] Y. A. Kosevich and E. S. Syrkin, Phys. Lett. A **135**, 298 (1989).
[15] Y. A. Kosevich, Progr. Surf. Sci. **55**, 1 (1997).
[16] B. Qiu and X. Ruan, Appl. Phys. Lett. **100**, 193101 (2012).
[17] Z.-Y. Ong and E. Pop, Phys. Rev. B **81**, 155408 (2010).
[18] S. Plimpton, J. Comput. Phys. **117**, 1 (1995).
[19] S. J. Stuart, A. B. Tutein, and J. A. Harrison, J. Chem. Phys. **112**, 6472 (2000).
[20] Y. Ni, H. L. Khanh, Y. Chalopin, J. B. Bai, P. Lebarny, L. Divay, and S. Volz, Appl. Phys. Lett. **100**, 193118 (2012).
[21] V. B. Shenoy, C. D. Reddy, A. Ramasubramaniam, and Y. W. Zhang, Phys. Rev. Lett. **101**, 245501 (2008).
[22] H. Zhao, K. Min, and N. R. Aluru, Nano Lett. **9**, 3012 (2009).
[23] S. Munetoh, T. Motooka, K. Moriguchi, and A. Shintani, Comput. Mater. Sci. **39**, 334 (2007).
[24] L. A. Girifalco, M. Hodak, and R. S. Lee, Phys. Rev. B **62**, 13104 (2000).
[25] L. Puech, G. Bonfait, and B. Castaing, J. Low Temp. Phys. **62**, 315 (1986).
[26] J.-L. Barrat and F. Chiaruttini, Mol. Phys. **101**, 1605 (2003).
[27] Y. Chalopin, K. Esfarjani, A. Henry, S. Volz, and G. Chen, Phys. Rev. B **85**, 195302 (2012).
[28] A. J. H. McGaughey and J. Li, *ASME 2006 International Mechanical Engineering Congress and Exposition, Heat Transfer, Vol. 1 Chicago, Illinois, USA* (ASME, Chicago, IL, 2006), pp. 317–325.
[29] See Supplemental Material at http://link.aps.org/supplemental/10.1103/PhysRevB.89.205413 for more information.
[30] S. G. Volz and G. Chen, Phys. Rev. B **61**, 2651 (2000).
[31] A. A. Balandin, Nat. Mater. **10**, 569 (2011).
[32] Y. Ni, Y. Chalopin, and S. Volz, Appl. Phys. Lett. **103**, 061906 (2013).
[33] Y. K. Koh, M.-H. Bae, D. G. Cahill, and E. Pop, Nano Lett. **10**, 4363 (2010).
[34] M. Freitag, M. Steiner, Y. Martin, V. Perebeinos, Z. Chen, J. C. Tsang, and P. Avouris, Nano Lett. **9**, 1883 (2009).
[35] K. F. Mak, C. H. Lui, and T. F. Heinz, Appl. Phys. Lett. **97**, 221904 (2010).
[36] Z. Chen, W. Jang, W. Bao, C. N. Lau, and C. Dames, Appl. Phys. Lett. **95**, 161910 (2009).
[37] Y. Ni, Y. Chalopin, and S. Volz, Appl. Phys. Lett. **103**, 141905 (2013).
[38] B. N. J. Persson and H. Ueba, Europhys. Lett. **91**, 56001 (2010).
[39] J. M. Dickey and A. Paskin, Phys. Rev. **188**, 1407 (1969).
[40] P. Heino, Eur. Phys. J. B **60**, 171 (2007).
[41] L. Lindsay, D. A. Broido, and N. Mingo, Phys. Rev. B **82**, 115427 (2010).
[42] M. M. Sadeghi, I. Jo, and L. Shi, Proc. Natl. Acad. Sci. USA **110**, 16321 (2013).
[43] R. L. Parc, C. Levelut, J. Pelous, V. Martinez, and B. Champagnon, J. Phys.: Condens. Matter **18**, 7507 (2006).
[44] G. Muller and M. Moser, *Handbook of Engineering Acoustics* (Springer, Berlin Heidelberg, 2013).
[45] S. Benchabane, A. Khelif, J. Y. Rauch, L. Robert, and V. Laude, Phys. Rev. E **73**, 065601 (2006).
[46] O. M. Braun and Y. S. Kivshar, *The Frenkel-Kontorova Model: Concepts, Methods, and Applications* (Springer-Verlag, Berlin, 2003).